

# Monitoring Wavepacket Dynamics at Conical Intersections by Entangled Two-Photon Absorption

Feng Chen,\* Bing Gu, and Shaul Mukamel\*

Cite This: <https://doi.org/10.1021/acsp Photonics.2c00255>

Read Online

ACCESS |



Metrics &amp; More



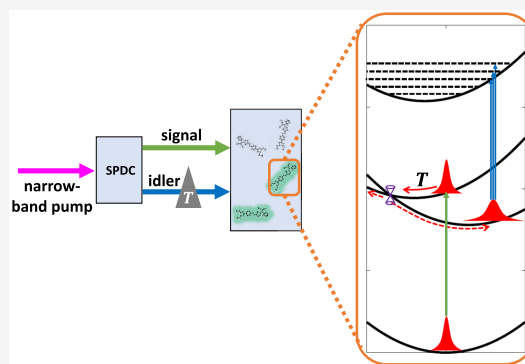
Article Recommendations



Supporting Information

**ABSTRACT:** In this theoretical study, we show how ultrafast electron–nuclear dynamics in a molecule can be monitored by two-photon absorption of time–energy entangled photon pairs generated by spontaneous parametric down-conversion with a narrow-band pump. The dynamics is tracked by a controllable signal-idler delay. Time correlation of the entangled photons enables an ultrafast measurement even with a monochromatic pump. The frequency anticorrelation of the photon pair allows the projection of the intermediate excited-state wavepacket onto an energy-selected vibrational level on a higher-lying electronic state with high energy resolution. Such joint high temporal and energy resolution is not possible with classical light. We demonstrate our scheme for a conical intersection model with four electronic states and two vibrational modes. The ultrafast nuclear wavepacket dynamics around the conical intersection is imprinted onto the time- and frequency-resolved entangled two-photon absorption signals. Electronic population dynamics is obtained by the frequency-integrated signal.

**KEYWORDS:** ultrafast nonlinear spectroscopy, molecules, temporal and spectral resolutions, spontaneous parametric down-conversion, nonadiabatic dynamics



Over the past two decades, novel quantum light spectroscopies<sup>1,2</sup> that utilize the quantum nature of light have been shown to possess some distinct advantages over their classical counterparts. For example, two-photon absorption of time–energy entangled photons contains many nonclassical features and functionalities,<sup>3–5</sup> including linear rather than quadratic scaling with the pump intensity,<sup>6–8</sup> observing classically forbidden transitions,<sup>9,10</sup> suppressing classical one-photon resonant peaks,<sup>11</sup> and manipulating excitation pathways.<sup>12,13</sup> A nearly 10 orders of magnitude enhancement of the two-photon absorption rate by entangled photons over classical light at the same photon fluxes has been reported,<sup>14–16</sup> thus reducing the risk of photodamage of biological samples. However, the magnitude of this enhancement has been questioned by recent experiments<sup>17–22</sup> and theoretical analysis.<sup>23,24</sup>

Entangled two-photon absorption (ETPA) has been applied for electronic state characterization<sup>25,26</sup> but so far has not been demonstrated for detecting electron–nuclear wavepacket dynamics. The passage through conical intersections (CIs)<sup>27</sup> is a ubiquitous example of ultrafast dynamics in molecules. CIs are degenerate sections of the adiabatic potential energy surfaces (PESs), around which the Born–Oppenheimer approximation breaks down and the nuclear and electronic motions become strongly coupled. Capturing the nonadiabatic dynamics at CIs constitutes a major challenge in ultrafast nonlinear spectroscopy. In some experimental techniques, the projections of the wavepacket onto chosen reference states are

observed. For example, in time-resolved fluorescence spectroscopy,<sup>28–30</sup> the excited-state wavepacket is projected onto the vibrational levels of the electronic ground state. In time-resolved photoelectron spectroscopy,<sup>31–33</sup> the wavepacket is mapped onto the continuum states of the ionized molecule and the ejected photoelectron. In both techniques, the temporal and spectral resolutions are determined by the duration and bandwidth of the pulse and are thus subjected to Fourier uncertainty.

Here, we introduce a variable delay between two entangled photons generated by spontaneous parametric down-conversion (SPDC) with a narrow-band pump (see Figure 1a). ETPA signals then monitor the wavepacket dynamics across a CI through the projection of the intermediate-state wavepacket onto an energy-selected vibrational level on a higher-lying electronic state (see Figure 1b). The nonclassical correlation between the entangled photons allows non-Fourier conjugated temporal and spectral resolution: the emission–time correlation allows ultrafast detection (even though the pump is narrow-band), and the frequency anticorrelation allows the

Received: February 14, 2022

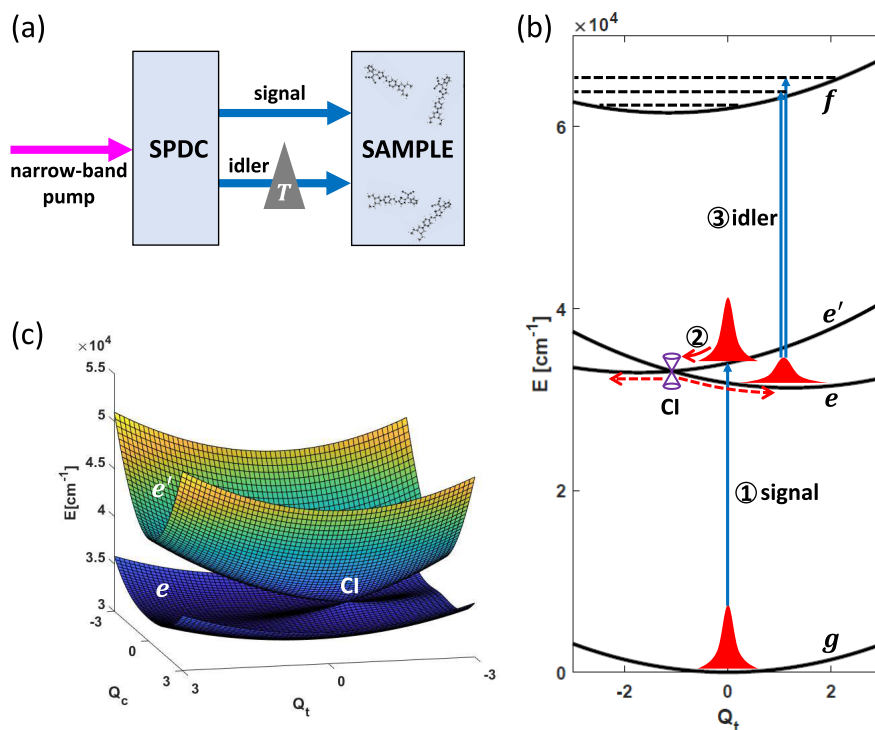


**Figure 1.** (a) Experimental setup for the proposed ETPA measurement of wavepacket dynamics in a molecule: a narrow-band pump photon is first split into two broadband photons (idler and signal) via a SPDC process; a controllable delay  $T$  is then introduced to the idler beam through a prism (gray triangle) that causes a phase shift; the two photons are finally directed to the molecular sample. (b) Molecular excitation process by the entangled photons prepared in (a): ① vertical excitation from  $g$  to  $e'$  by the signal photon; ② free evolution of the molecule for about time  $T$ ; ③ promotion of the wavepacket on  $e$  to a two-photon resonant vibrational level on  $f$ . The ETPA signal monitors the CI dynamics through the projection of the wavepacket on  $e$  onto an energy-selected vibrational eigenstate on  $f$ . By scanning the idler photon frequency, one gets a complete mapping of the wavepacket dynamics onto the vibrational manifold of  $f$ . Plotted is the cut through of the PESs of the molecule model along  $Q_c = 0$ . (c) PESs of  $e$  and  $e'$  and the CI between them. Parameters are  $\omega_{eg} = 31800 \text{ cm}^{-1}$ ,  $\omega_{e'g} = 34000 \text{ cm}^{-1}$ ,  $\omega_{fg} = 62000 \text{ cm}^{-1}$ ,  $\Omega_t = 697 \text{ cm}^{-1}$ ,  $\Omega_c = 1512 \text{ cm}^{-1}$ ,  $\kappa_e = -847 \text{ cm}^{-1}$ ,  $\kappa_{e'} = 1202 \text{ cm}^{-1}$ ,  $\kappa_f = 800 \text{ cm}^{-1}$ , and  $\lambda = 2110 \text{ cm}^{-1}$ .

selection of a two-photon resonant vibrational level on the electronic excited state. Entangled photons thus offer a powerful tool for monitoring ultrafast wavepacket dynamics.

The entangled photon pair produced by type-II SPDC with a monochromatic pump are described by the two-photon wave function:<sup>34,35</sup>

$$|\Phi\rangle = \int_0^\infty d\omega_i \int_0^\infty d\omega_s \phi(\omega_i, \omega_s) \hat{a}_i^\dagger(\omega_i) \hat{a}_s^\dagger(\omega_s) |\Omega\rangle \quad (1)$$

with

$$\phi(\omega_i, \omega_s) = \alpha_p \sqrt{\frac{T_e}{2}} \delta(\omega_i + \omega_s - \omega_p) \text{sinc}\left(\frac{\omega_i - \bar{\omega}_i}{2} T_e\right) e^{i\omega_i T} \quad (2)$$

where  $|\Omega\rangle$  is the vacuum state,  $|\alpha_p|^2$  is the photon flux (see Section S1 in Supporting Information),  $\omega_p$  is the pump frequency,  $\bar{\omega}_i$  and  $\bar{\omega}_s$  are the central frequencies of the idler and signal photons, which satisfy  $\bar{\omega}_i + \bar{\omega}_s = \omega_p$ , and  $T$  is an external delay applied to the idler beam. The entanglement time  $T_e$  represents the maximum mutual delay between the idler and signal photons at their generation.  $\hat{a}_j^\dagger(\omega)$  is the boson creation operator of the idler/signal ( $j = i, s$ ) photon with frequency  $\omega$ , satisfying  $[\hat{a}_j(\omega), \hat{a}_k^\dagger(\omega')] = \delta_{jk} \delta(\omega - \omega')$ . The Dirac delta function in eq 2 represents the frequency anticorrelation of the twin photons. The sinc function originates from phase matching of the SPDC process and gives rise to the signal-idler emission time correlation. This can

be directly seen by Fourier transform of the two-photon amplitude  $\phi(\omega_i, \omega_s)$  at  $T = 0$  into the time domain:

$$\tilde{\phi}(t_i, t_s) = \frac{\alpha_p}{2\pi\sqrt{2T_e}} \Pi\left(\frac{t_i - t_s}{T_e}\right) e^{-i\bar{\omega}_i t_i - i\bar{\omega}_s t_s} \quad (3)$$

where the rectangular function  $\Pi\left(\frac{t_i - t_s}{T_e}\right)$ , defined by  $\Pi(x) = 1$  for  $-1/2 < x < 1/2$  and 0 otherwise, imposes the constraint  $|t_i - t_s| \leq T_e/2$ . After introducing a delay  $T$  into the idler beam, the arrival times of the two photons on the sample satisfy  $T - T_e/2 \leq t_i - t_s \leq T + T_e/2$ .  $T_e$  thus sets the temporal resolution of the measurement. Our proposed scheme also applies to other phase-matching conditions (type-I and type-0), as it only relies on the time–energy entanglement.

Our molecular model consists of four diabatic electronic states ( $g, e, e'$ , and  $f$ ; see Figure 1b) and two vibrational modes (tuning mode  $t$ , and coupling mode  $c$ ) that are strongly coupled to the electronic motion and generate a conical intersection between  $e$  and  $e'$  (see Figure 1c). The molecular Hamiltonian in the diabatic representation reads

$$H_M = \sum_{\beta=t,c} \Omega_\beta \hat{b}_\beta^\dagger \hat{b}_\beta + \sum_{s=e,e',f} (\omega_{sg} + \kappa_s \hat{Q}_c) |s\rangle \langle s| + \lambda \hat{Q}_c (|e\rangle \langle e'| + |e'\rangle \langle e|) \quad (4)$$

where  $\hat{b}_\beta$  and  $\hat{b}_\beta^\dagger$  denote the boson annihilation and creation operators of the vibrational modes with the dimensionless

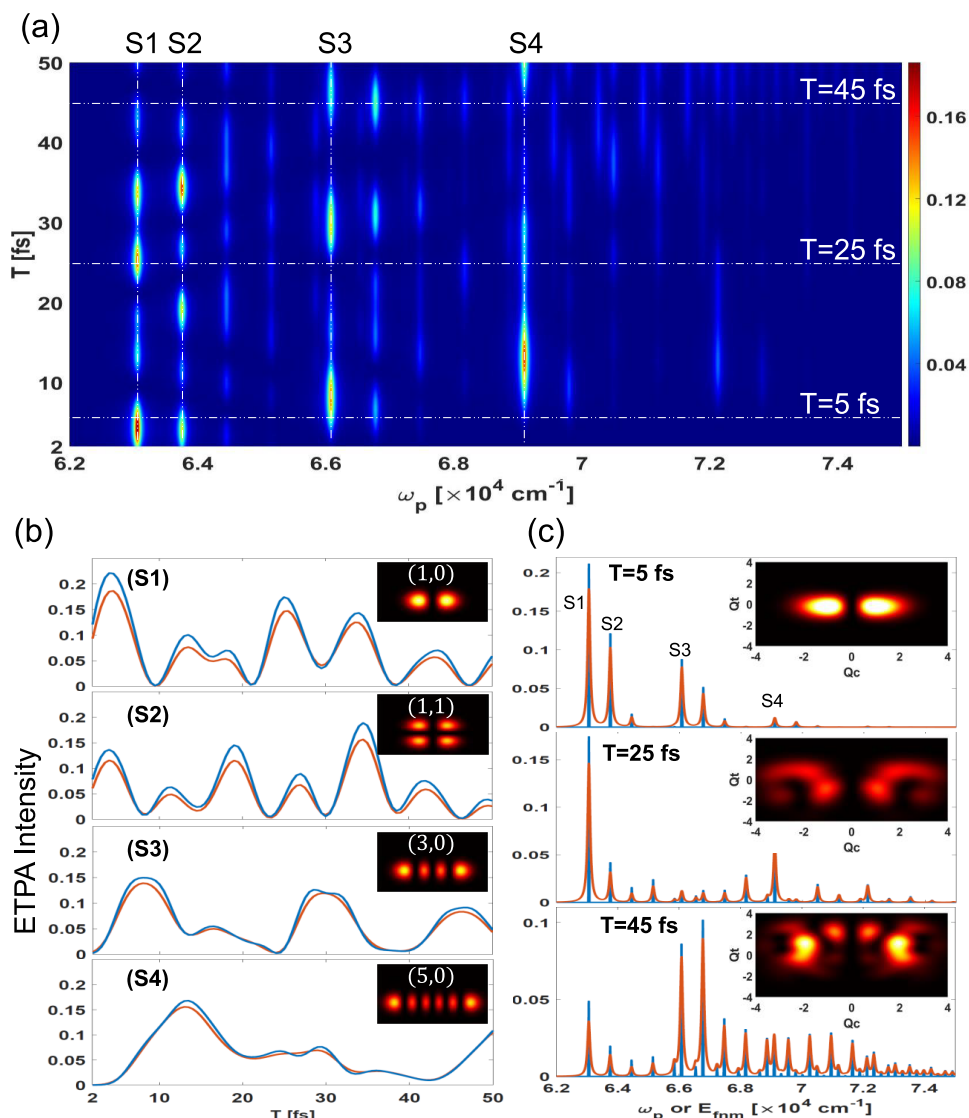


**Figure 2.** (a) 2D ETPA signal  $S(\omega_p, T)$  in eq 6 obtained by varying the signal-idler delay  $T$  and pump frequency  $\omega_p$ .  $T$  determines the wavepacket evolution time, and  $\omega_p$  selects the vibrational state onto which wavepacket is projected. The signal unit is  $CT_e^2 |\mu_{ef}^* \mu_{ge}^*|^2 / \gamma$  and  $\gamma = 50 \text{ cm}^{-1}$ . A short entanglement time ( $T_e = 4 \text{ fs}$ ) is chosen for high temporal resolution.  $T$  starts from 2 fs because we set the idler-signal delay no smaller than  $T_e/2$  to ensure that the idler photon always comes after the signal photon. (b) Comparison between ETPA signals (orange) along four vertical slices indicated in (a) and the projections of the wavepacket dynamics (blue) onto corresponding vibrational eigenstates on  $f$ :  $S(\omega_p = E_{fmm}, T)$  vs  $|\langle n, m_f | [\langle e | \Psi(T) \rangle]|^2$ . States are denoted  $(n, m_f)$ . The nuclear probability density for each vibrational eigenstate is shown in the inset. (c) Comparison between ETPA signals (orange) along three horizontal slices indicated in (a) and the distributions of wavepacket projections (blue) at three different evolution time:  $T = 5, 25$ , and  $45 \text{ fs}$ . The nuclear probability density of state  $e$  at each time is shown in the insets.

coordinates  $\hat{Q}_i$  and  $\hat{Q}_s$ ;  $\omega_{sg}$  is the vertical excitation energy at the Franck–Condon point from state  $g$  to  $s$ ;  $\kappa_s$  and  $\lambda$  are the intrastate and interstate electron-vibration coupling strength, respectively. The light–matter coupling in the interaction picture, under the dipole and rotating wave approximations, is given by  $H_I(t) = -\hat{\mu}^\dagger \hat{E}(t) - \hat{\mu} \hat{E}^\dagger(t)$ , where  $\hat{\mu} = \mu_{ge} |g\rangle\langle e'| + \mu_{ef} |e\rangle\langle f|$  is the lowering component of the dipole operator. We have assumed that the higher intermediate state  $e'$  is optically bright from the ground state  $g$ , whereas the lower intermediate state  $e$  is dark. The higher excited state  $f$  is dipole-coupled to  $e$  and  $g$  but not to  $e'$ . The dependence of  $\hat{\mu}$  on nuclear coordinates is neglected (Condon approximation). The positive-frequency component of the electric field operator is given by  $\hat{E}(t) = \hat{E}_i(t) + \hat{E}_s(t)$  with

$$\hat{E}_j(t) = \int_0^\infty d\omega \sqrt{\frac{\hbar\omega}{4\pi\epsilon_0 cA}} \hat{a}_j(\omega) e^{-i\omega t} \quad (5)$$

where  $c$  is the speed of light,  $\epsilon_0$  is the vacuum permittivity, and  $A$  is the effective area of the light beam.

The ETPA signal is defined as  $S(\omega_p, T) \equiv \frac{\dot{N}_f(t)}{\omega_p - \bar{\omega}_s}$ , where  $\dot{N}_f(t)$  is the growth rate of  $f$  state population that is measured through the fluorescence intensity from  $f$ , and the factor  $\frac{1}{\omega_p - \bar{\omega}_s}$  is chosen to keep the  $\omega_p$  dependence in a Lorentzian form (see eq 6). We have fixed  $\bar{\omega}_s = \omega_{e'g}$ , which can be achieved by tuning the phase matching conditions of the SPDC process. The signal is derived in Supporting Information, section S2 by

fourth-order time-dependent perturbation theory of the density matrix, resulting in

$$S(\omega_p, T) = \sum_{n,m_f} \frac{C\gamma}{(E_{fmm} - \omega_p)^2 + \gamma^2} \left| \int_{T-T_c/2}^{T+T_c/2} dt_1 \langle f | \otimes \langle n, m_f | \hat{\mu}^\dagger e^{-i(H_M - \bar{\omega}_s)t_1} \hat{\mu}^\dagger | g \rangle \otimes | 0, 0_g \rangle \right|^2 \quad (6)$$

where  $C = \frac{\hbar^2 |\alpha_p|^2 \bar{\omega}_s}{4T_c \epsilon_0^2 c^2 A^2}$ ,  $\gamma^{-1}$  is the  $f$  manifold vibronic states lifetime, and  $\langle n, m_f |$  stands for the product state of the  $n$ th vibrational eigenstate of the coupling mode and the  $m$ th vibrational eigenstate of the tuning mode on the  $f$  state PES. Similarly,  $|0, 0_g\rangle$  stands for the vibrational ground state on the  $g$  state PES.  $E_{fmm} = \omega_{fg} - \frac{k_f^2}{2\Omega_f} + n\Omega_c + m_f\Omega_t$  is the energy of the vibronic eigenstate  $|f\rangle \otimes |n, m_f\rangle$ . The Lorentzian prefactor in eq 6 indicates state selection by the pump frequency, and  $\gamma$  determines the energy resolution. We have neglected environment-induced relaxation effects, which is expected to limit state selectivity due to energy dissipation.

Equation 6 can be interpreted in the following two ways:

1. The integrand can be recast as

$$\begin{aligned} & \langle f | \otimes \langle n, m_f | \hat{\mu}^\dagger e^{-i(H_M - \bar{\omega}_s)t_1} \hat{\mu}^\dagger | g \rangle \otimes | 0, 0_g \rangle \\ &= \mu_{ef}^* \mu_{ge}^* \langle n, m_f | \langle e | e^{-i(H_M - \bar{\omega}_s)t_1} | e' \rangle \otimes | 0, 0_g \rangle \\ &= \mu_{ef}^* \mu_{ge}^* \langle n, m_f | \langle e | \Psi(t_1) \rangle \end{aligned} \quad (7)$$

where  $|\Psi(t_1)\rangle \equiv e^{-i(H_M - \bar{\omega}_s)t_1} |e'\rangle \otimes |0, 0_g\rangle$  is the nonstationary vibronic state of the molecule freely evolving under  $H_M - \bar{\omega}_s$  for time  $t_1$  after instantaneous vertical excitation from  $g$  to  $e'$ , and  $\langle e | \Psi(t_1) \rangle$  is the corresponding nuclear wavepacket on  $e$ . Therefore, apart from the constant prefactor, eq 7 is the projection of the nuclear wavepacket on  $e$  at time  $t_1$  onto the vibrational eigenstate  $|n, m_f\rangle$  on  $f$ , and the integral in eq 6 is the temporal average of this projection over the period  $[T - T_c/2, T + T_c/2]$ . Thus,  $|\Psi(T)\rangle$  is measured with time resolution  $T_c$ .

2. The integral in eq 6 can be alternatively recast as

$$\begin{aligned} & \int_{T-T_c/2}^{T+T_c/2} dt_1 \langle f | \otimes \langle n, m_f | \hat{\mu}^\dagger e^{-i(H_M - \bar{\omega}_s)t_1} \hat{\mu}^\dagger | g \rangle \otimes | 0, 0_g \rangle \\ &= \mu_{ef}^* \mu_{ge}^* e^{i\bar{\omega}_s T} \langle n, m_f | \left[ \langle e | e^{-iH_M T} \int_{-T_c/2}^{T_c/2} dt_1 e^{-i(H_M - \bar{\omega}_s)t_1} | e' \rangle \otimes | 0, 0_g \rangle \right] \\ &= \mu_{ef}^* \mu_{ge}^* e^{i\bar{\omega}_s T} \langle n, m_f | \langle e | e^{-iH_M T} |\tilde{\Psi}(0)\rangle \end{aligned} \quad (8)$$

where  $|\tilde{\Psi}(0)\rangle \equiv \int_{-T_c/2}^{T_c/2} dt_1 e^{-i(H_M - \bar{\omega}_s)t_1} |e'\rangle \otimes |0, 0_g\rangle$  is the nonstationary state created by a rectangular pulse with duration  $T_c$  and central frequency  $\bar{\omega}_s$ . The signal can thus be interpreted as the projections of the wavepacket precisely at time  $T$  after preparation by a rectangular pulse. In other words,  $|\tilde{\Psi}(T)\rangle = e^{-iH_M T} |\tilde{\Psi}(0)\rangle$  is probed with perfect time resolution.

The two interpretations of the signal come from the fact that the exact arrival time of each photon is indeterminate but the idler-signal time delay is known with uncertainty  $T_c$ , which can be interpreted as either ①  $t_1 \in [t_s + T - T_c/2, t_s + T + T_c/2]$  or ②  $t_s \in [t_1 - T - T_c/2, t_1 - T + T_c/2]$ . Hereafter, we adopt the

first interpretation and assume that we are detecting the wavepacket dynamics initiated by an impulsive excitation. Note that the temporal and spectral resolutions ( $T_c$  and  $\gamma$ ) of the measurement are not Fourier conjugates and thus not subjected to the Fourier uncertainty. This property stems from the fact that, although each photon of the pair is broadband, their frequency sum is well-defined.

The signal is calculated by exact diagonalization of  $H_M$  in the joint electron and nuclear Hilbert space. The occupation number basis is adopted for the vibrational degrees of freedom and converged results are achieved by truncating the Hilbert space at the maximum quantum number  $N_c = N_t = 30$ . Figure 2a shows the 2D ETPA signal obtained by scanning the delay  $T$  and the pump frequency  $\omega_p$ , holding  $\bar{\omega}_s$  fixed. We choose a short entanglement time ( $T_c = 4$  fs) to ensure good temporal resolution for ultrafast measurement of the wavepacket dynamics around the CI. The 2D signal constitutes a mapping of the wavepacket dynamics on  $e$  onto the  $f$  vibrational manifold. Signals appear along a set of vertical lines located at the  $f$ -manifold vibronic-state energies, i.e.,  $\omega_p = E_{fmm}$ . Note that state selection by classical short pulses ( $\sim 4$  fs) is not possible due to the broad bandwidth ( $\sim 4000$   $\text{cm}^{-1}$ ). In Figure 2b, we display four vertical slices of Figure 2a and find a good match with the simulated projections of wavepacket dynamics onto the corresponding vibrational states. The wavepacket dynamics leaves distinct fingerprints on different vibrational states. Figure 2c depicts three horizontal slices of Figure 2a for  $T = 5, 25$ , and  $45$  fs and again shows good agreement with the wavepacket simulations.

The frequency-integrated signal  $S^{\text{int}}(T)$  obtained by integrating  $S(\omega_p, T)$  over the pump frequency is given by (see Supporting Information, section S3 for the derivation)

$$\begin{aligned} S^{\text{int}}(T) &\equiv \int d\omega_p S(\omega_p, T) \\ &= C\pi |\mu_{ef}^* \mu_{ge}^*|^2 \langle \tilde{\Psi}(T) | (|e\rangle \langle e|) | \tilde{\Psi}(T) \rangle \\ &\approx C\pi T_c^2 |\mu_{ef}^* \mu_{ge}^*|^2 \langle \Psi(T) | \hat{N}_e | \Psi(T) \rangle \end{aligned} \quad (9)$$

with  $\hat{N}_e = |e\rangle \langle e|$ .  $S^{\text{int}}(T)$  is thus proportional to the  $e$ -state population at time  $T$  after the excitation. Figure 3 shows that  $S^{\text{int}}(T)$  for a short entanglement time follows closely the  $e$ -state population dynamics around the CI.

In summary, ETPA is shown to be a useful means for tracking ultrafast wavepacket dynamics without using ultra-short pulses. By scanning the signal-idler delay and the pump frequency, one obtains a dynamical mapping of the

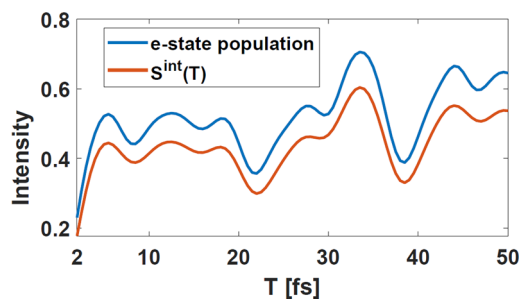


**Figure 3.** Frequency-integrated signal  $S^{\text{int}}(T)$  (eq 9) for  $T_c = 4$  fs follows closely the simulated  $e$ -state population dynamics. The unit of the signal intensity is  $C\pi T_c^2 |\mu_{ef}^* \mu_{ge}^*|^2$ .

intermediate state wavepacket onto the vibrational eigenstates of a higher-lying electronic state. The temporal and spectral resolutions of this measurement are not bound by Fourier uncertainty because they are not conjugates. Application to a model system undergoing a CI shows that the nonadiabatic dynamics are monitored by the ETPA signals and the electronic population change is captured by the frequency-integrated signal. A potential candidate to be studied with this technique is pyrazine,<sup>36</sup> which possesses a conical intersection between the first and second singlet excited states.

## ■ ASSOCIATED CONTENT

### SI Supporting Information

The Supporting Information is available free of charge at <https://pubs.acs.org/doi/10.1021/acsphotonics.2c00255>.

Derivation of the ETPA signal and the frequency-integrated ETPA signal (PDF)

## ■ AUTHOR INFORMATION

### Corresponding Authors

**Feng Chen** – Department of Chemistry and Department of Physics & Astronomy, University of California, Irvine, California 92697, United States; [orcid.org/0000-0001-8196-030X](https://orcid.org/0000-0001-8196-030X); Email: [chenf7@uci.edu](mailto:chenf7@uci.edu)

**Shaul Mukamel** – Department of Chemistry and Department of Physics & Astronomy, University of California, Irvine, California 92697, United States; [orcid.org/0000-0002-6015-3135](https://orcid.org/0000-0002-6015-3135); Email: [smukamel@uci.edu](mailto:smukamel@uci.edu)

### Author

**Bing Gu** – Department of Chemistry and Department of Physics & Astronomy, University of California, Irvine, California 92697, United States; [orcid.org/0000-0002-5787-3334](https://orcid.org/0000-0002-5787-3334)

Complete contact information is available at: <https://pubs.acs.org/10.1021/acsphotonics.2c00255>

### Funding

The support of NSF Grant No. CHE-1953045 is gratefully acknowledged. S.M. was supported by the U.S. Department of Energy, Office of Science, Office of Basic Energy Sciences under Award Number DE-SC0022134.

### Notes

The authors declare no competing financial interest.

## ■ REFERENCES

- (1) Dorfman, K. E.; Schlawin, F.; Mukamel, S. Nonlinear optical signals and spectroscopy with quantum light. *Rev. Mod. Phys.* **2016**, *88*, 045008.
- (2) Mukamel, S.; et al. Roadmap on quantum light spectroscopy. *J. Phys. B: At., Mol. Opt. Phys.* **2020**, *53*, 072002.
- (3) Gu, B.; Keefer, D.; Aleotti, F.; Nenov, A.; Garavelli, M.; Mukamel, S. Photoisomerization transition state manipulation by entangled two-photon absorption. *Proc. Natl. Acad. Sci. U. S. A.* **2021**, *118*, No. e2116868118.
- (4) Oka, H. Selective two-photon excitation of a vibronic state by correlated photons. *J. Chem. Phys.* **2011**, *134*, 124313.
- (5) Szoke, S.; Liu, H.; Hickam, B. P.; He, M.; Cushing, S. K. Entangled light–matter interactions and spectroscopy. *J. Mater. Chem. C* **2020**, *8*, 10732–10741.
- (6) Javanainen, J.; Gould, P. L. Linear intensity dependence of a two-photon transition rate. *Phys. Rev. A* **1990**, *41*, 5088–5091.

(7) Lee, D.-I.; Goodson, T. Entangled Photon Absorption in an Organic Porphyrin Dendrimer. *J. Phys. Chem. B* **2006**, *110*, 25582–25585.

(8) Georgiades, N. P.; Polzik, E. S.; Edamatsu, K.; Kimble, H. J.; Parkins, A. S. Nonclassical Excitation for Atoms in a Squeezed Vacuum. *Phys. Rev. Lett.* **1995**, *75*, 3426–3429.

(9) Gu, B.; Mukamel, S. Manipulating Two-Photon-Absorption of Cavity Polaritons by Entangled Light. *J. Phys. Chem. Lett.* **2020**, *11*, 8177–8182.

(10) Muthukrishnan, A.; Agarwal, G. S.; Scully, M. O. Inducing Disallowed Two-Atom Transitions with Temporally Entangled Photons. *Phys. Rev. Lett.* **2004**, *93*, 093002.

(11) Chen, F.; Mukamel, S. Entangled two-photon absorption with Brownian-oscillator fluctuations. *J. Chem. Phys.* **2022**, *156*, 074303.

(12) Schlawin, F.; Dorfman, K. E.; Fingerhut, B. P.; Mukamel, S. Suppression of population transport and control of exciton distributions by entangled photons. *Nat. Commun.* **2013**, *4*, 1782.

(13) Chen, F.; Mukamel, S. Vibrational Hyper-Raman Molecular Spectroscopy with Entangled Photons. *ACS Photonics* **2021**, *8*, 2722–2727.

(14) Villabona-Monsalve, J. P.; Varnavski, O.; Palfey, B. A.; Goodson, T. Two-Photon Excitation of Flavins and Flavoproteins with Classical and Quantum Light. *J. Am. Chem. Soc.* **2018**, *140*, 14562–14566.

(15) Tabakaev, D.; Montagnese, M.; Haack, G.; Bonacina, L.; Wolf, J.-P.; Zbinden, H.; Thew, R. T. Energy-time-entangled two-photon molecular absorption. *Phys. Rev. A* **2021**, *103*, 033701.

(16) Varnavski, O.; Pinsky, B.; Goodson, T. Entangled Photon Excited Fluorescence in Organic Materials: An Ultrafast Coincidence Detector. *J. Phys. Chem. Lett.* **2017**, *8*, 388–393.

(17) Landes, T.; Allgaier, M.; Merkouche, S.; Smith, B. J.; Marcus, A. H.; Raymer, M. G. Experimental feasibility of molecular two-photon absorption with isolated time-frequency-entangled photon pairs. *Phys. Rev. Research* **2021**, *3*, 033154.

(18) Parzuchowski, K. M.; Mikhaylov, A.; Mazurek, M. D.; Wilson, R. N.; Lum, D. J.; Gerrits, T.; Camp, C. H.; Stevens, M. J.; Jimenez, R. Setting Bounds on Entangled Two-Photon Absorption Cross Sections in Common Fluorophores. *Phys. Rev. Applied* **2021**, *15*, 044012.

(19) Mikhaylov, A.; Wilson, R. N.; Parzuchowski, K. M.; Mazurek, M. D.; Camp, C. H.; Stevens, M. J.; Jimenez, R. Hot-Band Absorption Can Mimic Entangled Two-Photon Absorption. *J. Phys. Chem. Lett.* **2022**, *13*, 1489–1493.

(20) Hickam, B. P.; He, M.; Szoke, S.; Cushing, S. Spectral and Temporal Measurement of Entangled Photon Interaction with a Virtual State Mediated Two-Photon Transition. *arXiv* **2022**; <https://arxiv.org/abs/2202.11764> (accessed 2022-03-24).

(21) Landes, T.; Allgaier, M.; Merkouche, S.; Smith, B. J.; Marcus, A. H.; Raymer, M. G. Experimental feasibility of molecular two-photon absorption with isolated time-frequency-entangled photon pairs. *Phys. Rev. Research* **2021**, *3*, 033154.

(22) Corona-Aquino, S.; Calderón-Losada, O.; Li-Gómez, M. Y.; Cruz-Ramirez, H.; Álvarez Venicio, V.; Carreón-Castro, M. d. P.; León-Montiel, R. J.; U'Ren, A. B. Experimental Study of the Validity of Entangled Two-Photon Absorption Measurements in Organic Compounds. *J. Phys. Chem. A* **2022**, *126*, 2185–2195.

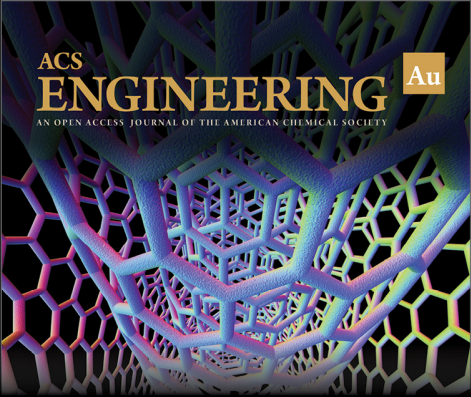
(23) Raymer, M. G.; Landes, T.; Marcus, A. H. Entangled two-photon absorption by atoms and molecules: A quantum optics tutorial. *J. Chem. Phys.* **2021**, *155*, 081501.

(24) Raymer, M. G.; Landes, T.; Allgaier, M.; Merkouche, S.; Smith, B. J.; Marcus, A. H. How large is the quantum enhancement of two-photon absorption by time-frequency entanglement of photon pairs? *Optica* **2021**, *8*, 757–758.

(25) Ishizaki, A. Probing excited-state dynamics with quantum entangled photons: Correspondence to coherent multidimensional spectroscopy. *J. Chem. Phys.* **2020**, *153*, 051102.

(26) Raymer, M. G.; Marcus, A. H.; Widom, J. R.; Vitullo, D. L. P. Entangled Photon-Pair Two-Dimensional Fluorescence Spectroscopy (EPP-2DFS). *J. Phys. Chem. B* **2013**, *117*, 15559–15575.

- (27) Yarkony, D. R. Diabolical conical intersections. *Rev. Mod. Phys.* **1996**, *68*, 985–1013.
- (28) Shah, J.; Damen, T. C.; Deveaud, B.; Block, D. Subpicosecond luminescence spectroscopy using sum frequency generation. *Appl. Phys. Lett.* **1987**, *50*, 1307–1309.
- (29) Sarkar, N.; Takeuchi, S.; Tahara, T. Vibronic Relaxation of Polyatomic Molecule in Nonpolar Solvent: Femtosecond Anisotropy/Intensity Measurements of the S<sub>n</sub> and S<sub>1</sub> Fluorescence of Tetracene. *J. Phys. Chem. A* **1999**, *103*, 4808–4814.
- (30) Braem, O.; Penfold, T. J.; Cannizzo, A.; Chergui, M. A femtosecond fluorescence study of vibrational relaxation and cooling dynamics of UV dyes. *Phys. Chem. Chem. Phys.* **2012**, *14*, 3513–3519.
- (31) Von Conta, A.; Tehlar, A.; Schletter, A.; Arasaki, Y.; Takatsuka, K.; Wörner, H. J. Conical-intersection dynamics and ground-state chemistry probed by extreme-ultraviolet time-resolved photoelectron spectroscopy. *Nat. Commun.* **2018**, *9*, 3162.
- (32) Stolow, A.; Bragg, A. E.; Neumark, D. M. Femtosecond Time-Resolved Photoelectron Spectroscopy. *Chem. Rev.* **2004**, *104*, 1719–1758.
- (33) Horio, T.; Spesyvtsev, R.; Nagashima, K.; Ingle, R. A.; Suzuki, Y.-i.; Suzuki, T. Full observation of ultrafast cascaded radiationless transitions from S<sub>2</sub>( $\pi\pi^*$ ) state of pyrazine using vacuum ultraviolet photoelectron imaging. *J. Chem. Phys.* **2016**, *145*, 044306.
- (34) Keller, T. E.; Rubin, M. H. Theory of two-photon entanglement for spontaneous parametric down-conversion driven by a narrow pump pulse. *Phys. Rev. A* **1997**, *56*, 1534–1541.
- (35) Fedrizzi, A.; Herbst, T.; Aspelmeyer, M.; Barbieri, M.; Jennewein, T.; Zeilinger, A. Anti-symmetrization reveals hidden entanglement. *New J. Phys.* **2009**, *11*, 103052.
- (36) Woywod, C.; Domcke, W.; Sobolewski, A. L.; Werner, H. Characterization of the S<sub>1</sub>–S<sub>2</sub> conical intersection in pyrazine using ab initio multiconfiguration self-consistent-field and multireference configuration-interaction methods. *J. Chem. Phys.* **1994**, *100*, 1400–1413.



ACS  
**ENGINEERING** Au  
AN OPEN ACCESS JOURNAL OF THE AMERICAN CHEMICAL SOCIETY

Editor-in-Chief: **Prof. Shelley D. Minteer**, University of Utah, USA

 Deputy Editor:  
**Prof. Vivek Ranade**  
University of Limerick, Ireland

**Open for Submissions** 

pubs.acs.org/engineeringau  ACS Publications  
Most Trusted. Most Cited. Most Read.

# SI: Monitoring Wavepacket Dynamics at Conical Intersections by Entangled Two-photon Absorption

Feng Chen,<sup>\*</sup> Bing Gu, and Shaul Mukamel<sup>\*</sup>

*Department of Chemistry and Department of Physics & Astronomy, University of California, Irvine, CA 92697, USA*

E-mail: chenf7@uci.edu; smukamel@uci.edu

## S1 Photon flux and entangled two-Photon wavefunction

In order to derive the relation between photon flux and prefactor of the entangled two-photon wavefunction under cw pump, we first study the photon flux of a Gaussian-shape coherent pulse described by  $|\alpha\rangle$ , satisfying  $\hat{a}(\omega)|\alpha\rangle = \alpha(\omega)|\alpha\rangle$  and  $\alpha(\omega) = \alpha_0(2\pi\sigma^2)^{-1/4}e^{-(\omega-\omega_p)^2/4\sigma^2}$ .

Then the photon flux satisfies<sup>1</sup>

$$\begin{aligned}\sqrt{I_p(t)} &= \int_0^\infty \frac{d\omega}{\sqrt{2\pi}} \alpha(\omega) e^{-i(\omega-\omega_p)t} \\ &= (2/\pi)^{1/4} \alpha_0 \sigma^{1/2} e^{-\sigma^2 t^2}.\end{aligned}\tag{S1}$$

For cw light,  $\sqrt{I_p} \xrightarrow{\sigma \rightarrow 0} (2/\pi)^{1/4} \alpha_0 \sigma^{1/2}$ .

Now we consider the entangled two-photon state pumped by the a Gaussian-pulse with

the same duration  $1/\sigma$ , which is described by

$$|\Phi\rangle = \epsilon \int d\omega_i d\omega_s \Phi(\omega_i, \omega_s) \hat{a}_i(\omega_i) \hat{a}_s(\omega_s) |\Omega\rangle, \quad (\text{S2})$$

where  $\Phi(\omega_i, \omega_s) = \phi_B(\omega_i) \phi_N(\omega_i + \omega_s - \omega_p)$  with normalized functions

$$\begin{aligned} \phi_B(\omega_i) &= \sqrt{\frac{T_e}{2\pi}} \text{sinc}\left(\frac{\omega_i - \bar{\omega}_i T_e}{2}\right) \\ \phi_N(\omega_i, \omega_s) &= (2\pi\sigma^2)^{-1/4} e^{-(\omega_i + \omega_s - \omega_p)/4\sigma^2} \\ &\stackrel{\sigma \rightarrow 0}{\equiv} (2\pi\sigma^2)^{-1/4} \sqrt{4\pi\sigma} \delta(\omega_i + \omega_s - \omega_p). \end{aligned} \quad (\text{S3})$$

We impose that the coherent light and entangled photon state have the same number of photons:  $2\epsilon^2 = \alpha_0^2$ .<sup>1</sup> As a result, their photon fluxes are also identical. Combining Eq. (S1-S3), we can now write Eq. S2 as

$$|\Phi\rangle = \sqrt{I_p T_e / 2} \int d\omega_i d\omega_s \text{sinc}\left(\frac{\omega_i - \bar{\omega}_i T_e}{2}\right) \delta(\omega_i + \omega_s - \omega_p) \hat{a}_i(\omega_i) \hat{a}_s(\omega_s) |\Omega\rangle, \quad (\text{S4})$$

## S2 Derivation of the ETPA signal

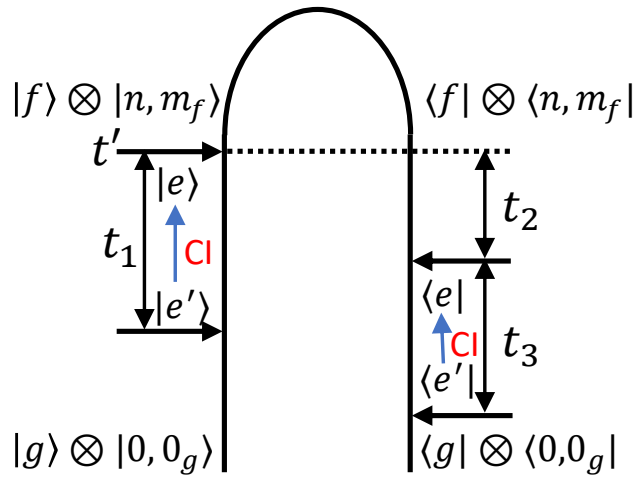


Figure S1: Loop diagram for ETPA. Incoming arrows denote photon absorptions. For diagrammatic rules, see Ref. 2.

The loop diagram for the ETPA signal is given in Fig. S1, from which one gets

$$\begin{aligned}
N_f(t) &= \int_{-\infty}^t dt' \int_0^{\infty} dt_{1\sim 3} \langle g | \otimes \langle 0, 0_g | \hat{\mu}(t' - t_2 - t_3) \hat{\mu}(t' - t_2) \hat{\mu}^\dagger(t') \hat{\mu}^\dagger(t' - t_1) | g \rangle \otimes | 0, 0_g \rangle \\
&\quad \times \langle \Phi | \hat{E}^\dagger(t' - t_2 - t_3) \hat{E}^\dagger(t' - t_2) \hat{E}(t') \hat{E}(t' - t_1) | \Phi \rangle + \text{h.c.}
\end{aligned} \tag{S5}$$

Thus, the  $f$  state populating rate is

$$\begin{aligned}
&\frac{d}{dt} N_f(t) \\
&= 2\text{Re} \int_0^{\infty} dt_{1,2,3} \langle g | \otimes \langle 0, 0_g | \hat{\mu}(t_1) \hat{\mu}(t_1 + t_3) \hat{\mu}^\dagger(t_1 + t_2 + t_3) \hat{\mu}^\dagger(t_2 + t_3) | g \rangle \otimes | 0, 0_g \rangle \\
&\quad \times \langle \Phi | \hat{E}^\dagger(t_1) \hat{E}^\dagger(t_1 + t_3) \hat{E}(t_1 + t_2 + t_3) \hat{E}(t_2 + t_3) | \Phi \rangle \\
&= 2\text{Re} \sum_{n,m_f} \int_0^{\infty} dt_{1,2,3} \langle \Phi | \hat{E}^\dagger(0) \hat{E}^\dagger(t_3) | 0 \rangle \langle 0 | \hat{E}(t_1) \hat{E}(0) | \Phi \rangle e^{i(E_{fnm} + i\gamma - \omega_P)t_2 + i\omega_P(t_1 - t_3)} \\
&\quad \times \langle g | \otimes \langle 0, 0_g | \hat{\mu} e^{iH_M t_3} \hat{\mu} | f \rangle \otimes | n, m_f \rangle \langle f | \otimes \langle n, m_f | \hat{\mu}^\dagger e^{-iH_M t_1} \hat{\mu}^\dagger | g \rangle \otimes | 0, 0_g \rangle \\
&= \sum_{n,m_f} \left| \int_0^{\infty} dt_1 \langle f | \otimes \langle n, m_f | \hat{\mu}^\dagger e^{-iH_M t_1} \hat{\mu}^\dagger | g \rangle \otimes | 0, 0_g \rangle \langle 0 | \hat{E}(t_1) \hat{E}(0) | \Phi \rangle e^{i\omega_P t_1} \right|^2 \\
&\quad \times \frac{2\gamma}{(E_{fnm} - \omega_P)^2 + \gamma^2},
\end{aligned} \tag{S6}$$

where  $\gamma$  is the natural linewidth of  $f$  state and  $\langle n, m_f |$  stands for the product state of the  $n$ -th vibrational eigenstate of  $c$  mode and the  $m$ -th vibrational eigenstate of  $t$  mode taking into account the nuclei displacement of the PES minimum of  $f$ . Similarly,  $|0, 0_g\rangle$  stands for the vibrational ground state of  $g$  state.  $E_{fmn} = E_f - \frac{k_f^2}{2\omega_t} + n\omega_c + m_f\omega_t$  is the energy of the vibronic eigenstate  $|f\rangle \otimes |n, m_f\rangle$ . Using Eq. (1) and (5) in the main text, one has

$$\langle 0 | \hat{E}(t_1) \hat{E}(0) | \Phi \rangle = \frac{\hbar\alpha_P}{2\sqrt{2}\epsilon_0 c A} \sqrt{\frac{\bar{\omega}_i \bar{\omega}_s}{T_e}} \Pi\left(\frac{t_1 - T}{T_e}\right) e^{-i\bar{\omega}_i(t_1 - T)}, \tag{S7}$$

where we have applied the slowly varying envelope approximation and assumed that the

external delay  $T$  is longer than the entanglement time  $T_e$  such that the idler photon arrives at the sample later than the signal photon. Plug the above equation into Eq. S6, one has

$$\begin{aligned} \frac{d}{dt} N_f(t) &= \frac{\hbar^2 \alpha_P^2 \bar{\omega}_s (\omega_P - \bar{\omega}_s)}{4 T_e \epsilon_0^2 c^2 A^2} \sum_{n, m_f} \frac{\gamma}{(E_{fnm} - \omega_P)^2 + \gamma^2} \\ &\times \left| \int_{T-T_e/2}^{T+T_e/2} dt_1 \langle f | \otimes \langle n, m_f | \hat{\mu}^\dagger e^{-i(H_M - \bar{\omega}_s)t_1} \hat{\mu}^\dagger | g \rangle \otimes |0, 0_g \rangle \right|^2, \end{aligned} \quad (\text{S8})$$

### S3 Derivation of the frequency-integrated ETPA signal

The frequency-integrated signal  $S^{\text{int}}(T)$  is defined by integrating over the pump-frequency at each time delay:

$$\begin{aligned} S^{\text{int}}(T) &= \int d\omega_P S(\omega_P, T) \\ &= C\pi \sum_{n, m_f} \left| \int_{T-T_e/2}^{T+T_e/2} dt_1 \langle f | \otimes \langle n, m_f | \hat{\mu}^\dagger e^{-i(H_M - \omega_{e'g})t_1} \hat{\mu}^\dagger | g \rangle \otimes |0, 0_g \rangle \right|^2 \\ &= C\pi |\mu_{ef}^* \mu_{ge'}^*|^2 \sum_{n, m_f} \int_{T-T_e/2}^{T+T_e/2} dt_{1,2} \langle e' | \otimes \langle 0, 0_g | e^{i(H_M - \omega_{e'g})t_2} | e \rangle \otimes |n, m_f \rangle \\ &\quad \times \langle e | \otimes \langle n, m_f | e^{-i(H_M - \omega_{e'g})t_1} | e' \rangle \otimes |0, 0_g \rangle \\ &= C\pi |\mu_{ef}^* \mu_{ge'}^*|^2 \int_{T-T_e/2}^{T+T_e/2} dt_{1,2} \langle e' | \otimes \langle 0, 0_g | e^{i(H_M - \omega_{e'g})t_2} | e \rangle \langle e | e^{-i(H_M - \omega_{e'g})t_1} | e' \rangle \otimes |0, 0_g \rangle \\ &= C\pi |\mu_{ef}^* \mu_{ge'}^*|^2 \langle \tilde{\Psi}(T) | (|e\rangle \langle e|) | \tilde{\Psi}(T) \rangle \\ &\approx C\pi T_e^2 |\mu_{ef}^* \mu_{ge'}^*|^2 \langle e' | \otimes \langle 0, 0_g | e^{iH_M T} | e \rangle \langle e | e^{-iH_M T} | e' \rangle \otimes |0, 0_g \rangle \\ &= C\pi T_e^2 |\mu_{ef}^* \mu_{ge'}^*|^2 \langle \Psi(T) | (|e\rangle \langle e|) | \Psi(T) \rangle, \end{aligned} \quad (\text{S9})$$

where  $|\tilde{\Psi}(T)\rangle$  and  $|\Psi(T)\rangle$  are defined in the main text.

## References

- (1) Raymer, M. G.; Landes, T.; Marcus, A. H. Entangled two-photon absorption by atoms and molecules: A quantum optics tutorial. *J. Chem. Phys.* **2021**, *155*, 081501, Publisher: American Institute of Physics.
- (2) Marx, C. A.; Harbola, U.; Mukamel, S. Nonlinear optical spectroscopy of single, few, and many molecules: Nonequilibrium Green's function QED approach. *Phys. Rev. A* **2008**, *77*, 022110.